An SPIM-FEM coupling strategy for damage modelling

Samir S. Saliba[1], Lapo Gori[1], Roque L. S. Pitangueira[1]

[1]*Structural Engineering Department, Federal University of Minas Gerais*
Avenida Antônio Carlos, 6627, 31270-901, Belo Horizonte/MG, Brazil
samirsaliba@yahoo.com, lapo@dees.ufmg.br, roque@dees.ufmg.br

Abstract. This paper proposes a coupling strategy between the finite element method (FEM) and meshfree methods belonging to the family of Smoothed Point Interpolation Methods (SPIMs), to analyse two-dimensional problems with scalar damage. Starting from a model that is fully discretised by the FEM, the proposed strategy is capable to identify the regions where nonlinear phenomena occour, and to convert the FEM mesh to an SPIM discretisation in such regions, in order to obtain a coupled FEM-SPIM model. When the FEM mesh is replaced, the SPIM discretisation is built using the original FEM nodes and additional nodes, in order to improve the approximation in the nonlinear regions. The characteristics of the proposed approach are illustrated with a set of numerical simulations, comparing the results of the coupled model with the results of full FEM and SPIM models.

Keywords: Smoothed Point Interpolation Methods, Finite element method, Coupling, Scalar damage

1 Introduction

The finite element method (FEM) is one of the most important numerical methods employed in structural analysis due its stability, efficiency and accuracy. However, it is a mesh-dependent method, and it can present some drawbacks in some kind of analyses. On the other hand, meshfree methods build their approximation functions in terms of nodes, and this feature facilitate the discretisation of the domain. These methods however, usually are more computationally expensive that the standard FEM.

There are different types of meshfree methods in the literature. According to Belytschko et al. [1], the stating point of meshfree was the smoothed particle hydrodynamics (SPH) method, presented by Gingold and Monaghan [2] and Lucy [3] in 1977. From this point on, many other methods were developed, as the element free Galerkin (EFG) method, proposed by Belytschko et al. [4], the point interpolation method (PIM), proposed by Liu and Gu [5] and the smoothed point interpolation methods (SPIM) developed by Liu and Zhang [6].

In an attempt to take advantage of the qualities of FEM and meshfree methods, several researchers proposed to couple them, and the present work proposes an automated coupling between the FEM and the SPIM, aiming to model two-dimensional problems with scalar damage. The SPIM will substitute the FEM based on the singularity of the acoustic tensor and additional nodes will be added in order to improve the meshfree approximation. To illustrate this approach numerical simulations are presented, in order to point out the behaviour when compared to full FEM and meshfree models.

2 Smoothed point interpolation methods

The displacement field $u(\mathbf{x})$ at a point $\mathbf{x}$, in meshfree methods, can be approximated as

$$u(\mathbf{x}) = \sum_{i=1}^{n} \phi_i(\mathbf{x}) u_i, \tag{1}$$

where n is the number of nodes, ϕ_i is the nodal shape function and u_i is the nodal displacement.

SPIM strategies use point interpolation methods (PIM), based on polynomial or radial basis functions (RBF), to construct the shape functions. Liu and Gu [5] developed the method using polynomial functions, referred to as PIM. Wang and Liu [7] proposed the use of radial basis, resulting in the radial point interpolation method (RPIM).

Liu and Gu [8] and Wang and Liu [9] combined both basis and formulated the radial point interpolation method with polynomial reproduction (RPIMp). The three shape functions are obtained from an interpolation resulting in the Kronecker delta property, making it possible a direct imposition of the essential boundary conditions.

2.1 RPIM

Equation 1 can be rewritten using the RPIM as

$$u(\mathbf{x}) = \begin{bmatrix} \mathbf{R}^T(\mathbf{x}) & \mathbf{p}^T(\mathbf{x}) \end{bmatrix} \mathbf{G}^{-1} \begin{bmatrix} \mathbf{u} \\ \mathbf{0} \end{bmatrix}, \tag{2}$$

where the shape function $\phi(\mathbf{x}) = \begin{bmatrix} \mathbf{R}^T(\mathbf{x}) & \mathbf{p}^T(\mathbf{x}) \end{bmatrix} \mathbf{G}^{-1}$, $\mathbf{R}$ is the radial basis functions, $\mathbf{p}$ is the monomials of the polynomial base and $\mathbf{G}$ is the combined moment matrix.

In this work the following exponential radial function was adopted to build the radial basis functions:

$$R_i(r_i) = \exp\left(-c\, r_i^2\right), \tag{3}$$

where $r_i = \sqrt{(x - x_i)^2 + (y - y_i)^2}$ is the distance between x and the node i, and c is the shape parameter.

2.2 Smoothing domains construction

SPIM strategies are based on smoothed derivatives, which are calculated using the concept of smoothing domains [6]. To construct them the problem domain is divided into a set of smoothing domains, which are usually created using triangular background cells. The smoothing domains must satisfy two requirements: they must cover the entire problem domain, and there must be no gaps or overlaps between them. Different SPIM models can be constructed based on: nodes (NS-PIM) [10], edges (ES-PIM) [11] or cells (CS-PIM) [12], as shown in Fig. 1.

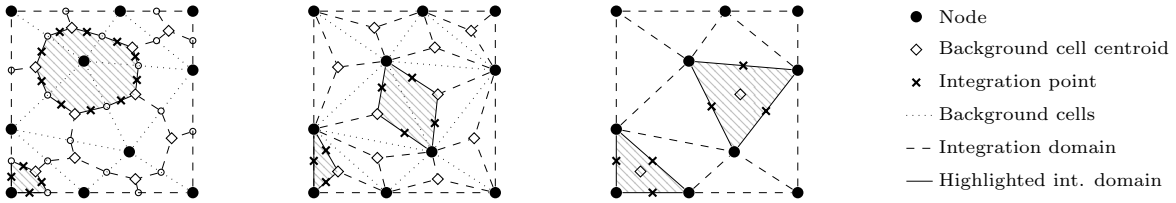

(a) Node-based (b) Edge-based (c) Cell-based

Figure 1. Smoothing domains

2.3 T-schemes for nodes selection

The same background cells used to build the smoothing domains can also be used to select the nodes of the support domain at each integration point. Triangular background cells are usually adopted in SPIM strategies, thus allowing the use of the so-called T-schemes.

Among the various existing schemes, this work focuses on the following: T3 scheme, edge-based T4 scheme (or simply T4 scheme, from now on), and T6/3 scheme. They are illustrated in Fig. 2, where the different colours indicate the support nodes for the highlighted integration point.

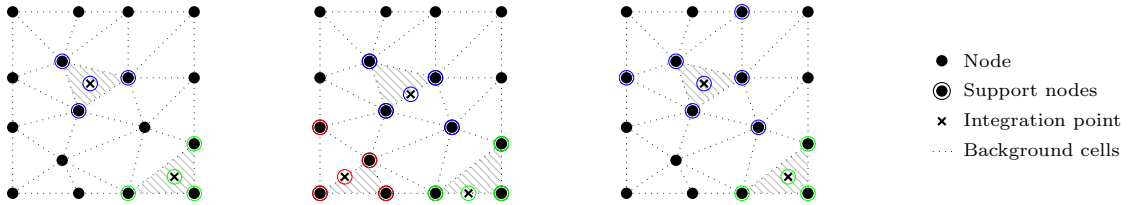

(a) T3 scheme (b) T4 scheme (c) T6/3 scheme

Figure 2. Local support nodes using T-schemes

3 Automated coupling of finite element and meshfree methods

The automated coupling method relies on the singularity of the acoustic tensor to identify the nonlinear regions that will be converted to SPIM. The SPIM discretisations are built considering the original FEM nodes and additional nodes, in order to improve the approximation in the nonlinear regions.

3.1 SPIM-FEM coupling

The key point of every coupling strategy is to guarantee the compatibility of the approximation in the transition zone. In the case of SPIM methods, the coupling can be performed directly, because the FEM and SPIM shape functions possess the Kronecker delta property. A similar approach was proposed in a paper by Zhang et al. [13], coupling the RPIM with FEM. Figure 3 illustrate a simplified one-dimensional coupling between FEM and RPIMp [14].

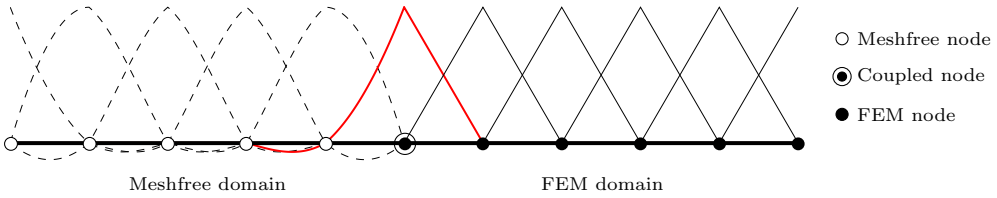

Figure 3. Coupled shape functions - RPIMp-FEM

3.2 Acoustic tensor

The acoustic tensor is given by

$$\mathbf{Q} = (\mathbf{n} \cdot \mathbf{E} \cdot \mathbf{n}), \tag{4}$$

where $\mathbf{n}$ is a normal unit vector and $\mathbf{E}$ is the constitutive tensor.

Usually to determine the initial formation of a weak discontinuity, the singularity of acoustic tensor is employed. Thus, the eq. (4) can be rewritten by

$$det(\mathbf{Q}) = det(\mathbf{n} \cdot \mathbf{E} \cdot \mathbf{n}) = 0. \tag{5}$$

Using this approach it's possible to detect regions that should be converted to SPIM due to the onset of nonlinear phenomena. It's worth it to note that the singularity of the acoustic tensor is detected at the single integration points. In order to avoid the substitution of just one element at the time, when the singularity is detected for a certain element, all the elements within a certain region are also replaced by an SPIM discretisation. The elements that must be replaced are the ones that fall within a circular region centered at the centroid of the detected element. The radius of such region is assumed to be equal to the average size of the detected element multiplied by a scale factor, which in this work as been assumed as 2. More details regarding the numerical evaluation of the singularity of the acoustic tensor can be found in the work by Fioresi [15].

4 Scalar damage models

The behaviour of quasi-brittle materials during a loading-unloading process can be described with elastic-degrading models, where the material elastic properties progressively degrades as the strains exceed certain threshold values. A feature of these models is the existence of a total relationship between stresses and strains, which can be expressed by

$$\boldsymbol{\sigma} = \hat{\mathbf{E}}^S \boldsymbol{\varepsilon}, \qquad \boldsymbol{\varepsilon} = (\hat{\mathbf{E}}^S)^{-1} \boldsymbol{\sigma}, \tag{6}$$

where $\boldsymbol{\sigma}$ is the stress tensor, $\boldsymbol{\varepsilon}$ is the strain tensor and $\hat{\mathbf{E}}^S$ is the secant constitutive operator. Disregarding the micro cracks closure-reopening effects, the secant operator remains constant within an unloading-reloading process.

Among the different elastic-degrading models, scalar damage models are the simpler ones. Their secant constitutive operator is expresses by [16–18]

$$\hat{\mathbf{E}}^S(D, \hat{\mathbf{E}}^0) = (1 - D)\hat{\mathbf{E}}^0, \tag{7}$$

where D is a scalar damage variable, assumed to vary from 0 (undamaged material) to 1 (completely damaged material), and $\hat{\mathbf{E}}^0$ is the initial constitutive operator. For a scalar damage model, a common choice for the loading

function is represented by the following additive decomposition

$$f(\boldsymbol{\varepsilon}, D) = \varepsilon_{eq}(\boldsymbol{\varepsilon}) - K(D) \leqslant 0, \tag{8}$$

where $\varepsilon_{eq}(\boldsymbol{\varepsilon})$ is an equivalent strain, and $K(D)$ is a historical parameter that is representative of the maximum level of strain reached during the loading process. The damage variable is usually prescribed as a function of the equivalent strain; in this work the following exponential damage law is being adopted

$$D(\varepsilon_{eq}) = 1 - \frac{K_0}{\varepsilon_{eq}}(1 - \alpha + \alpha e^{-\beta(\varepsilon_{eq} - K_0)}), \tag{9}$$

where K_0 is a threshold value for the equivalent strain, and α and β are parameters that define the maximum allowed damage level and the damage evolution intensity, respectively. In this work, the Mazars scalar damage model [19, 20] was considered, and the equivalent deformation is given by

$$\varepsilon_{eq} = \sqrt{\left[\sum_{k=1}^{3}(< \varepsilon^{(k)} >_+)^2\right]}, \tag{10}$$

where $\varepsilon^{(k)}$ is the kth eigenvalue of the strain tensor and $< \varepsilon^{(k)} >_+ = (\varepsilon^{(k)} + |\varepsilon^{(k)}|)/2$ its positive part.

5 Numerical simulations

The present section points out two different numerical simulations, a L-shaped panel and a three point bending test. These simulations illustrate the automated FEM-SPIM coupling and compare the results with models completely discretised by FEM or SPIM over the entire domain (or simply full FEM and full SPIM, from now on).

All the full FEM models were discretised with three-nodes triangular elements, and these meshes were adopted as background cells for the construction of the meshfree discretisations. The meshfree shape functions were constructed with the RPIMp using the exponential radial function (eq. (3)) with $c = 0.002$ and 3 polynomial terms. The support nodes were selected using T4 scheme for cell-based models, and the T3 and T6/3 schemes for node- and edge-based models. The system of nonlinear equations was solved by the Newton-Raphson method, together with the displacement control method, adopting as control point the node where the force F is applied, and controlling its vertical displacement. All simulations were performed using the secant approximation of the constitutive operator.

5.1 L-shaped panel

Figure 4a illustrates the L-shaped panel and Fig. 4b shows the discretisation used in these analyses. This panel has a thickness of 100 mm and it is subjected to a reference load $F = 7000$ N. A vertical displacement increment of 7.5×10^{-4} mm, and a tolerance of 1.0×10^{-4} for the convergence in displacement were adopted. The same material parameters presented by Winkler et al. [21] were adopted here: $E = 25850$ MPa and $\nu = 0.18$. The nonlinear behaviour was reproduced with the exponential damage law of eq. (9), with: $\alpha = 0.95$, $\beta = 1100$ and $K_0 = 1.12 \times 10^{-4}$.

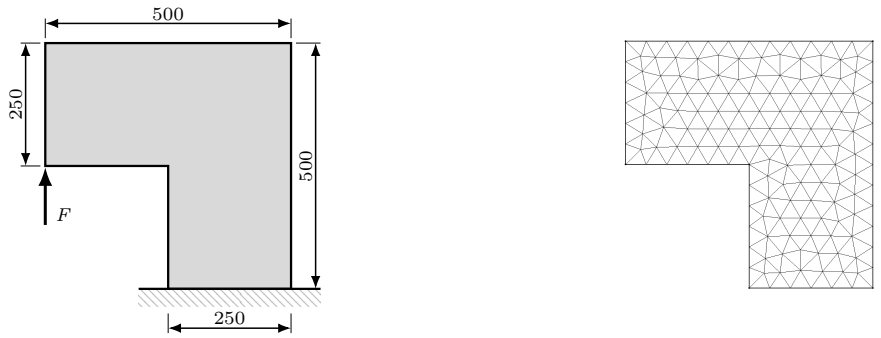

(a) Geometry (measures in mm) (b) Discretisation

Figure 4. L-shaped panel

The results are illustrated in Fig. 5, where the vertical displacement of the control point is plotted against the load factor. As it can be seen, the coupled models improve the behaviour of the full meshfree models in the

softening branch, the cell and edge-based methods presented the results a little bit softening than experimental test, but the maximum load was very close for both, this branch for the coupled models was influenced for both methods, improving the node-based substantially. The linear branch of the coupled models is governed to the FEM, because the first change of FEM to SPIM occour in approximately 0.75 of the load factor. As expected, the region substituted for SPIM at the end of simulation, presented in the Fig. 6, is where the test present the higher damage values, based on this it is possible understand the improvement obtained in the coupled models when compared with full models. Another interesting point is regarding the T6/3 scheme, that for the edge-based coupled model continuous similar to full model and for the node-base coupled model the equilibrium path was close to T3 scheme.

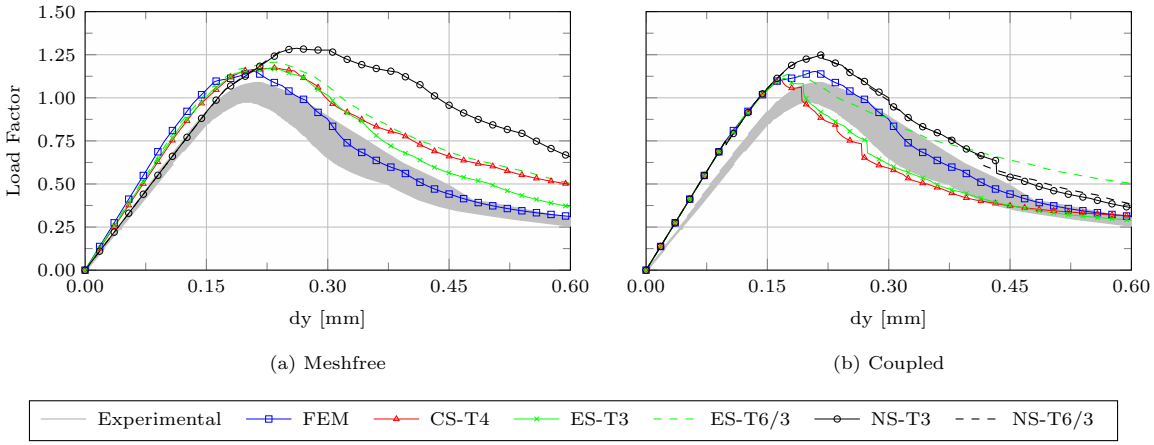

Figure 5. L-shaped panel - Equilibrium paths

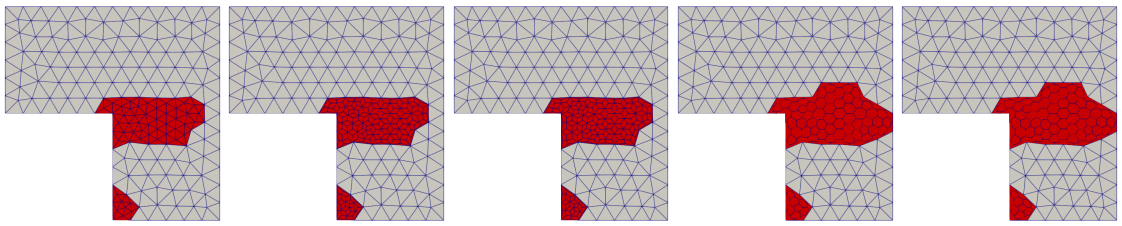

(a) CS (b) ES-T3 (c) ES-T6/3 (d) NS-T3 (e) NS-T6/3

Figure 6. L-shaped panel - Final meshes of coupled models

5.2 Three-point bending test

The beam illustrated in Fig. 7a has a thickness of 50 mm and it is subjected to a reference load $F = 800$ N. The discretisation employed to perform the simulations is presented in Fig. 7b, and the material parameters was adopted from a paper by Petersson [22]: $E = 30000$ MPa and $\nu = 0.2$. The nonlinear behaviour was reproduced with the exponential damage law of eq. (9), with: $\alpha = 0.95$, $\beta = 1100$ and $K_0 = 1.1 \times 10^{-4}$. A vertical displacement increment of -5×10^{-3} mm, and a tolerance of 1.0×10^{-4} for the convergence in displacement were employed.

In this simulation, the full cell and edge-base models with T3-scheme reproduced the experimental test very well, however the full node-based models didn't present good results, as happened in the section 5.1. The coupled models improve the results again, mainly for node-based models, that presented a equilibrium path very close to the experimental test. The maximum load of the cell and edge-based coupled models was similar to the one of the experimental test and the linear branch for all coupled models was governed by the FEM, while the softening branch was governed by both FEM and SPIM. Figure 9 points out the last configuration obtained in the coupled models, where again the meshfree region is located where happened the higher damage values.

6 Conclusions

This work presented an automated coupling between the FEM and the SPIM models to study physically nonlinear problems with scalar damage. The automated coupling approach was used to reproduce two experimental test and the obtained results were compared with full FEM and SPIM models. In both simulations the coupled

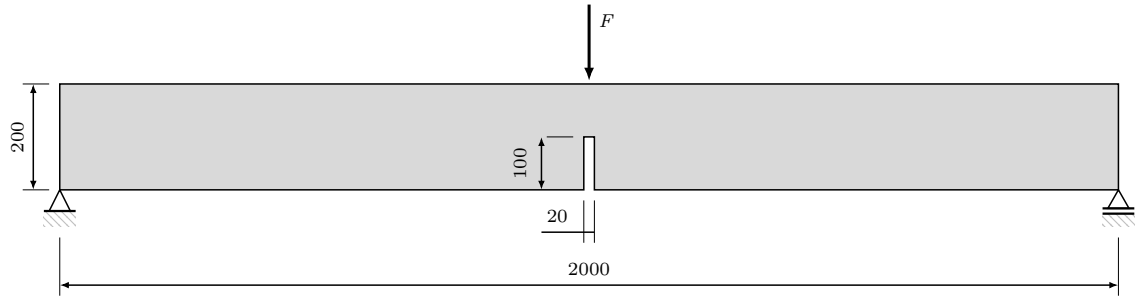

(a) Geometry (measures in mm)

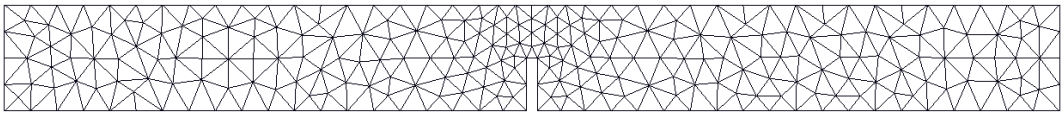

(b) Discretisation

Figure 7. Three-point bending

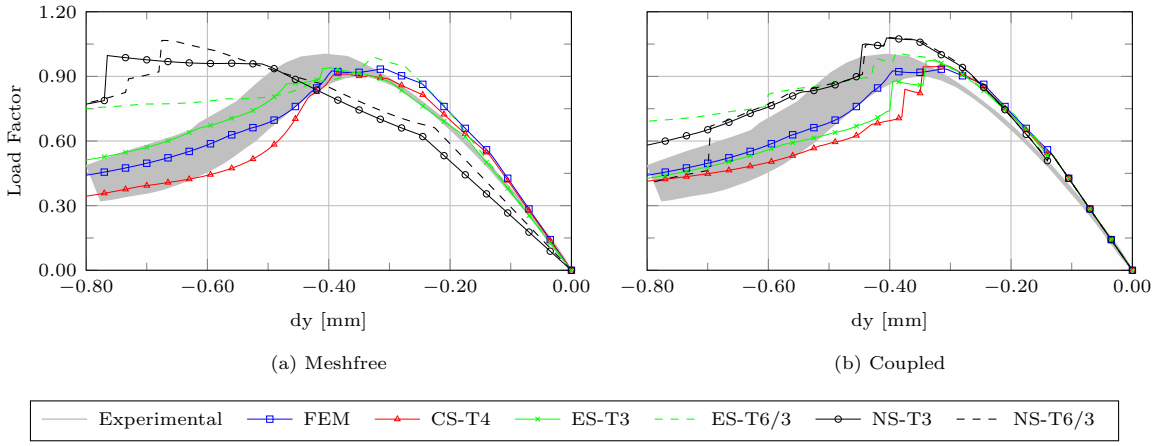

Figure 8. Three-point bending - Equilibrium paths

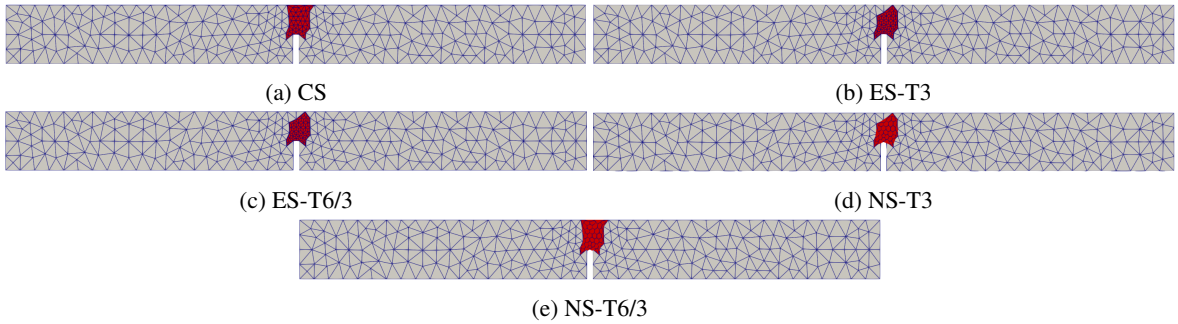

(a) CS (b) ES-T3

(c) ES-T6/3 (d) NS-T3

(e) NS-T6/3

Figure 9. Three-point bending - Final meshes of coupled models

models presented results in good agreement with the expected experimental results. The linear branch of the two simulations in the coupled models was governed by the FEM, because the conversion of FEM to SPIM happened just above the middle of the branch. For the node-based models, the coupling considerably improved the results in both the simulations, mainly in the softening branch. The T6/3 scheme presented results a little more rigid in the softening branch independent of the model. In particular, the automated coupling models adopted in this work was capable to improve the behaviour of the full meshfree models independent of the T-scheme applied. Anyway, the authors believe that this approach can open another possibilities for further researches.

Acknowledgements. The authors gratefully acknowledge the support from the Brazilian research agencies CAPES (Coordenação de Aperfeiçoamento de Pessoal de Nível Superior), FAPEMIG (Fundação de Amparo à Pesquisa do

Estado de Minas Gerais; grant PPM-00747-18), and CNPq (Conselho Nacional de Desenvolvimento Científico e Tecnológico; grant 309515/2017-3).

Authorship statement. The authors hereby confirm that they are the sole liable persons responsible for the authorship of this work, and that all material that has been herein included as part of the present paper is either the property (and authorship) of the authors, or has the permission of the owners to be included here.

References

[1] T. Belytschko, Y. Krongauz, D. Organ, M. Fleming, and P. Krysl. Meshless methods: An overview and recent developments. *Computer Methods in Applied Mechanics and Engineering*, vol. 139, pp. 3–47, 1996.
[2] R. A. Gingold and J. J. Monaghan. Smoothed particle hydrodynamics: theory and application to non-spherical stars. *Mon. Not. Roy. Astron. Soc.*, vol. 181, pp. 375–389, 1977.
[3] B. L. Lucy. A numerical approach to the testing of the fission hypothesis. *The Astronomical Journal*, vol. 82, n. 12, pp. 1013–1024, 1977.
[4] T. Belytschko, Y. Y. Lu, and L. Gu. Element-free galerkin methods. *International Journal for Numerical Methods in Engineering*, vol. 37, pp. 229–256, 1994.
[5] G. R. Liu and Y. T. Gu. A point interpolation method for two-dimensional solids. *International Journal for Numerical Methods in Engineeringb*, vol. 50, n. 4, pp. 937–951, 2001a.
[6] G. R. Liu and G. Y. Zhang. *Smoothed point interpolation methods - G space theory and weakened weak forms*. World Scientific Publishing Co. Pte. Ltd., USA, 2013.
[7] J. G. Wang and G. R. Liu. Radial point interpolation method for elastoplastic problems. In *Proceedings of the First International Conference on Structural Stability and Dynamics*, pp. 703–708, Taipei, Taiwan, 2000.
[8] G. R. Liu and Y. T. Gu. A local radial point interpolation method (lrpim) for free vibration analyses of 2-d solids. *Journal of Sound and Vibration*, vol. 246, n. 1, pp. 29–46, 2001b.
[9] J. G. Wang and G. R. Liu. A point interpolation meshless method based on radial basis functions. *International Journal for Numerical Methods in Engineering*, vol. 54, n. 11, pp. 1623–1648, 2002.
[10] G. R. Liu, G. Y. Zhang, K. Y. Dai, Y. Y. Wang, Z. H. Zhong, G. Y. Li, and X. Han. A linearly conforming point interpolation method (lc-pim) for 2d solid mechanics problems. *International Journal of Computational Methods*, vol. 2, n. 4, pp. 645–665, 2005.
[11] G. R. Liu and G. Y. Zhang. Edge-based smoothed point interpolation methods. *International Journal of Computational Methods*, vol. 5, n. 4, pp. 621–646, 2008.
[12] G. R. Liu and G. Y. Zhang. A normed g space and weakened weak (W^2) formulation of a cell-based smoothed point interpolation method. *International Journal of Computational Methods*, vol. 6, n. 1, pp. 147–179, 2009.
[13] Y. Zhang, J. Wang, and B. Zhang. Coupled fem and meshless radial point interpolation method. *Journal of Tsinghua University (Science and Technology)*, vol. 48, n. 6, pp. 951–954, 2008.
[14] S. S. Saliba, L. Gori, and R. L. S. Pitangueira. A coupled finite element-meshfree smoothed point interpolation method for nonlinear analysis. *Engineering Analysis with Boundary Elements*, vol. 128, pp. 1–18, 2021.
[15] L. A. F. Fioresi. Análise de localização de deformações em modelos fisicamente não lineares. Master's thesis, Escola de Engenharia de Estruturas da Universidade Federal de Minas Gerais, Belo Horizonte, Brasil, 2019.
[16] I. Carol, E. Rizzi, and K. Willam. A unified theory of elastic degradation and damage based on a loading surface. *International Journal of Solids and Structures*, vol. 31, pp. 2835–2865, 1994.
[17] S. S. Penna. *Formulação Multipotencial para Modelos de Degradação Elástica: Unificação Teórica, Proposta de Novo Modelo, Implementação Computacional e Modelagem de Estruturas de Concreto*. PhD thesis, Escola de Engenharia de Estruturas da Universidade Federal de Minas Gerais, Belo Horizonte, Brasil, 2011.
[18] L. Gori, S. S. Penna, and R. L. S. Pitangueira. A computational framework for constitutive modelling. *Computers and Structures*, vol. 187, pp. 1–23, 2017.
[19] J. Mazars. *Application de le Mécanique de l'endommagement au comportement non lineaire et à la rupture du béton de Structure*. PhD thesis, Université Pierre et Marie Curie - Laboratoire de Mécanique et Technologie, Paris, France (in french), 1984.
[20] de R. Borst and M. A. Gutiérrez. A unified framework for concrete damage and fracture models including size effects. *International Journal of Fracture*, vol. 95, pp. 261–277, 1999.
[21] B. Winkler, G. Hofstetter, and H. Lehar. Application of a constitutive model for concrete to the analysis of a precast segmental tunnel lining. *International Journal for Numerical and Analytical Methods in Geomechanics*, vol. 28, n. 7-8, pp. 797–819, 2004.
[22] P. Petersson. *Crack growth and development of fracture zones in plain concrete and similar materials*. PhD thesis, Tech. Rep. TVBM-1006, Division of Building Materials, Lund Institute of Technology, Lund, Sweden, 1981.